Quasiclassical Trajectory Simulations of Pyrazine−Argon and Methylpyrazine−Argon van der Waals Cluster Predissociation and Collisional Energy Transfer†

Laurie M. Yoder and John R. Barker*

Department of Chemistry and Department of Atmospheric, Oceanic and Space Sciences, University of Michigan, Ann Arbor, Michigan 48109-2143

Received: March 31, 2000; In Final Form: May 26, 2000

Vibrational energy transfer in van der Waals cluster predissociation and in collisions between aromatic molecules (pyrazine and methylpyrazine) and argon was investigated by means of quasiclassical trajectory calculations. The calculated results for cluster predissociation show that only a small fraction of the available vibrational energy is transferred to recoil energy, and the recoil energy distribution can be described by a smooth, roughly exponential function, in good agreement with experimental data [Yoder, L. M.; Barker, J. R. *Phys. Chem. Chem. Phys.* **2000**, *2*, 813]. The calculated collisional step-size distributions are almost independent of temperature for $T \leq 300$ K, but change in a complicated way for $T > 300$ K. It is also found that the cluster dissociation energy transfer distributions resemble those of low-temperature collisions.

Introduction

In van der Waals (vdW) clusters, the flow of energy is hindered by inefficient coupling between the high-frequency molecular vibrational modes and the low-frequency vdW modes. Characteristics that change the coupling between these groups of modes enhance or hinder vibrational energy transfer in the cluster. Some of these characteristics include the initial vibrational energy, the density of states of the donor molecule, in-plane or out-of-plane mode character and the vdW well depth. To investigate some of these variables, recent experiments[1,2] have focused on determination of the product recoil energy following vibrational predissociation of vdW dimers. In these experiments, the clusters consisted of an aromatic molecule and either a rare gas atom or another molecule. The aromatic member of the cluster was excited to 2500−8500 cm^{-1} vibrational energy in the first triplet state (T_1) by way of intersystem crossing from the first excited singlet state (S_1). Following dissociation of the cluster, the recoil distribution of the aromatic member was monitored. In each case, the recoil energy distribution is a smooth, nearly exponential function, peaked at zero recoil. The average recoil energy is not strongly dependent on either the initial excitation energy or the presence of a methyl rotor on the aromatic partner.

The smooth and structureless recoil distributions suggest that classical mechanics may qualitatively describe the dynamics, even though the average vibrational energy per mode is less than one quantum at these vibrational energies (2500−8500 cm^{-1}). The density of states of the aromatic molecule is large ($\rho = 10^3-10^6$ states/cm^{-1}), however, and the average recoil energy is only a small fraction (<3% for argon) of the initial excitation energy. Thus, conservation of zero point energy should not be a consideration.

The main questions we address in this work are: (1) How well can classical trajectory calculations simulate vibrational predissociation? and (2) How are cluster predissociation and collisional energy transfer related?

Trajectory calculations are a useful tool in the study of collisional energy transfer. They allow the controlled study of the effects of potential surface, vibrational energy, collision duration, and temperature on the dynamics of energy exchange. Through calculations, cluster lifetime and rotational energy transfer, which are not available experimentally, can be analyzed. In this work, classical trajectories are used to simulate the energy transfer between vibrationally excited pyrazine and argon in both vdW clusters and collisions. The focus is on the overall qualitative trends regarding the temperature and vibrational energy dependence of collisional energy transfer. To this end, only a simple pairwise Lennard-Jones intermolecular potential is used. The quantitative accuracy of the calculation is determined by the details of the potential, and other studies have explored these effects.[3−5]

The link between "full collisions" and vibrational predissociation of clusters, or "half collisions" is pursued through the temperature dependence of collisional energy transfer. In both experimental[6−9] and trajectory[5,10,11] studies, the temperature dependence of collisional energy transfer has been shown to be weak. To the extent that collisional processes and vibrational predissociation can be described by the same interaction potential surface, a "half collision" corresponds to a full collision that occurs at low rotational and translational temperature. In the limit of low temperature, the energies of translations and rotations approach zero, which is the initial condition for dissociation of a vdW cluster.

Theory

The classical equations of motion were integrated using the public domain program VENUS96.[12] The same potential energy surface was used for both the cluster dissociation and collisional trajectories. The pyrazine and methylpyrazine intramolecular potential surfaces consisted of Morse stretches, harmonic bends, wags, and torsions. This valence force field included only interactions between adjacent atoms; interactions between atoms not directly bonded to each other were neglected. These potential types are standard options in VENUS96, and have been frequently applied in other classical trajectory studies of energy transfer.[4,5,10,13] The benzene force constants used by Lenzer et al.[5] were modified to achieve reasonable agreement between

† Part of the special issue "C. Bradley Moore Festschrift".

10.1021/jp001248d CCC: $19.00
Published on Web 07/06/2000

TABLE 1: Intramolecular Potential Parameters for Pyrazine and 2-Methylpyrazine

Morse stretching terms	exponential constant ($Å^{-1}$)	equilibrium bond length (Å)	bond strength (kcal/mol)
aromatic C−N	1.999	1.340	130.0
aromatic C−C	1.918	1.403	130.0
C−CH_3	1.330	1.489	100.0
aromatic C−H	1.808	1.115	110.0
methyl C−H	1.800	1.112	90.0
harmonic bending terms	force constant (mdyn Å rad^{-2})	equilibrium bond angle	
aromatic N−C−C	1.165	122.5°	
aromatic C−N−C	1.155	115.0°	
aromatic N−C−C at CH_3 substitution	1.140	116.0°	
N−C−H	0.521[a]	116.0°	
N−C−CH_3	0.912	117.9°	
methyl C−C−H	0.667[b]	109.471°	
methyl H−C−H	0.561[b]	109.471°	
harmonic wagging terms	force constant (mdyn Å rad^{-2})	equilibrium geometry	
C−C−H out-of-plane wag pyrazine	0.353	planar	
C−C−H out-of-plane wag methylpyrazine	0.303	planar	
C−C−CH_3	0.20	planar	
torsional terms	barrier height (kcal/mol)		
aromatic C−C bond: pyrazine	15.8		
aromatic N−C bond: pyrazine	18.0		
aromatic C−C bond: methylpyrazine	22.0		
aromatic N−C bond: methylpyrazine	24.0		
methyl rotor	1.15		

[a] Reference 5. [b] Reference 4.

TABLE 2: Experimental and Calculated Vibrational Frequencies

Calculated Vibrational Frequencies for Pyrazine
353, 419, 522, 606, 648, 784, 865, 941, 1005, 1046, 1047, 1076, 1118, 1242, 1264, 1314, 1544, 1665, 1741, 1761, 3032, 3034, 3035, 3036

Experimental Vibrational Frequencies for Pyrazine[a]
350, 418, 602, 704, 756, 785, 927, 960, 983, 1016, 1018, 1063, 1130, 1149, 1233, 1346, 1411, 1483, 1525, 1580, 3012, 3040, 3055, 3069

Calculated Vibrational Frequencies for Methylpyrazine
222, 235, 369, 376, 456, 497, 560, 622, 719, 774, 942, 970, 973, 1022, 1028, 1083, 1134, 1222, 1233, 1337, 1460, 1475, 1478, 1527, 1691, 1738, 1752, 2654, 2762, 2764, 3034, 3036, 3036

Experimental Vibrational Frequencies for Methylpyrazine[b]
169, 207, 356, 406, 466, 560, 636, 748, 790, 814, 830, 840, 931, 977, 1020, 1060, 1156, 1176, 1249, 1303, 1377, 1399, 1447, 1450, 1477, 1528, 1581, 2927, 2965, 3008, 3037, 3057, 3071

[a] Reference 14. [b] Reference 15.

the calculated and experimental[14] vibrational frequencies of the ground electronic state of pyrazine. Methylpyrazine[15,16] parameters were adapted from the toluene parameters of Lim.[4] Even though the molecules contain significant vibrational energy, the average energy per mode is small. The low-frequency modes of the molecule are most important in energy transfer, and good agreement between the calculated and experimental low-frequency values was of high priority in choosing the force constants. The force constants used in this work are listed in Table 1, and the calculated and experimental vibrational frequencies are compared in Table 2. Good agreement is obtained for the pyrazine low-frequency modes, while the middle frequency modes are represented less well.

The intermolecular potential function was composed of atom−atom pairwise Lennard-Jones potentials with toluene−Ar parameters[17] for C−Ar and H−Ar interactions. The N−Ar interaction was obtained by scaling the C−Ar interaction as in ref 18. These parameters are shown in Table 3. This potential (Figure 1) predicts the deepest potential wells to be ∼3.2 Å above and below the center of the ring with a well depth of 700 cm^{-1}. This well depth is close to 738 cm^{-1}, the deepest well of benzene−Ar.[19] The shallower in-plane potential wells differ slightly from those of benzene because of the lower

TABLE 3: Intermolecular Potential Parameters

	$V = (A/r^{12}) - (B/r^6)$	
interaction	A (kcal mol^{-1} $Å^{12}$)	B (kcal mol^{-1} $Å^6$)
C−Ar[a]	1.190×10^6	1.179×10^3
N−Ar	9.044×10^5	1.060×10^3
H−Ar[a]	2.250×10^5	3.260×10^2

[a] Reference 17.

symmetry of pyrazine. The two in-plane minima located beside the pyrazine C−C bonds are shallower than their benzene counterparts[19] (276 cm^{-1} compared with 297 cm^{-1}) and the four in-plane wells located beside the C−N bonds are slightly more stable (318 cm^{-1}). Even with their minor differences in symmetry and numbers of H atoms, the intermolecular surfaces of pyrazine−Ar and benzene−Ar are similar enough that the resulting calculations are comparable, given the same initial conditions.

van der Waals Clusters. Zero point energy was included in all of the modes. The initial vibrational excitation energy in excess of the zero point energy was placed in the high-frequency C−H stretching modes. This was done to simulate the experiment in which the cluster is prepared by intersystem crossing from S_1 to T_1.[1,2] The high-frequency modes are expected to be

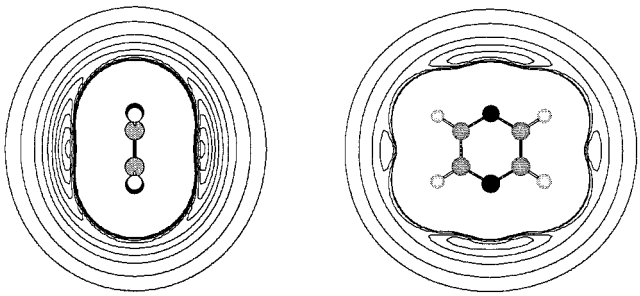

Figure 1. Potential energy surface for Ar interaction with pyrazine. Slices are shown through the surface perpendicular to the plane of the molecule and in the plane of the molecule. The outer contour is −0.1 kcal/mol, subsequent contours are −0.2 to −1.8 kcal/mol in increments of 0.2 kcal/mol.

the most important acceptors for the vibrational energy in this transition.[20] Additional calculations were performed with the excess vibrational energy distributed among different groups of pyrazine modes, but the final recoil distributions were not sensitive to the initial vibrational distribution. The integration step sizes were 0.1 and 0.05 fs for pyrazine−Ar and methylpyrazine−Ar, respectively, to conserve total energy to within ± 0.7 cm^{-1}. Approximately 3000 trajectories were calculated at each excitation energy (4000 and 8500 cm^{-1} above the zero-point energy). These energies correspond to the S_1-T_1 energy splitting for pyrazine[21] and benzene,[22] respectively. The cluster lifetimes were analyzed for a sample of approximately half of the trajectories. Each trajectory was terminated when the separation between cluster fragments was 16 Å. At this separation, there is essentially no interaction between the cluster partners. For ∼1000 trajectories or more, the average energy disposal converged to within 2%.

Pyrazine−Ar Collisions. The initial vibrational energy (4000, 8500, or 24000 cm^{-1} in addition to the zero-point energy) was distributed microcanonically among the vibrational modes of the pyrazine molecule. The initial rotational and translational energies were sampled from thermal distributions at 75, 150, 300, 700, or 1000 K. Throughout this paper, the "temperature" of the collision refers to the initial rotational and translational energy distributions. This is distinct from the microcanonical vibrational excitation energy, which is not in thermal equilibrium with the rotations or translations. The impact parameters (b) were sampled from the appropriate statistical distribution ranging from 0 to b_{max}.[23] The maximum impact parameter (b_{max}) was chosen so that there was essentially no contribution to the energy transfer at $b > b_{max}$. The value chosen for b_{max} is temperature dependent: b_{max} (75 K, 150 K) = 12 Å, b_{max} (300 K) = 9 or 10 Å, b_{max} (700 K) = 9 Å, b_{max} (1000 K) = 8 Å. The temperature variation is due to the attractive vdW potential at long range. The value of b_{max} is important in the determination of a collision frequency, which is used to scale the results to a per collision basis. This will be addressed further in the Results and Discussion section. For each temperature, 30 000 trajectories were calculated. The large number of trajectories was necessary to obtain good statistics for energy transfer events of low probability. The initial separation distance of the collision partners was 18 Å between the argon atom and one nitrogen atom, and each trajectory was integrated until the separation was 20 Å. These distances are larger than those for the cluster studies to allow for different initial orientations in the collisions.

Results and Discussion

Pyrazine−Ar Cluster Dissociation. The dynamics of the cluster predissociation was first investigated by animating individual trajectories and looking for qualitative trends. In a typical trajectory, the excited pyrazine molecule vibrates as the energy initially contained in the high frequency stretches randomizes throughout the other modes. The low frequency vdW modes do not couple effectively with the molecular modes, so energy transfer between them is slow. After many vibrational periods, the vdW bend and stretch modes become excited and the argon atom leaves the deep potential well above the plane of the pyrazine molecule. The argon atom "hops" around on the pyrazine surface, sampling the shallow in-plane potential minima, as well as the other deep well centered above the opposite face of the ring (Figure 1). Eventually the argon atom receives a "kick" and recoils from the pyrazine molecule. The dissociation kick and subsequent recoil take place over a very short time compared to the total trajectory duration, so we identify the cluster lifetime with the trajectory duration.

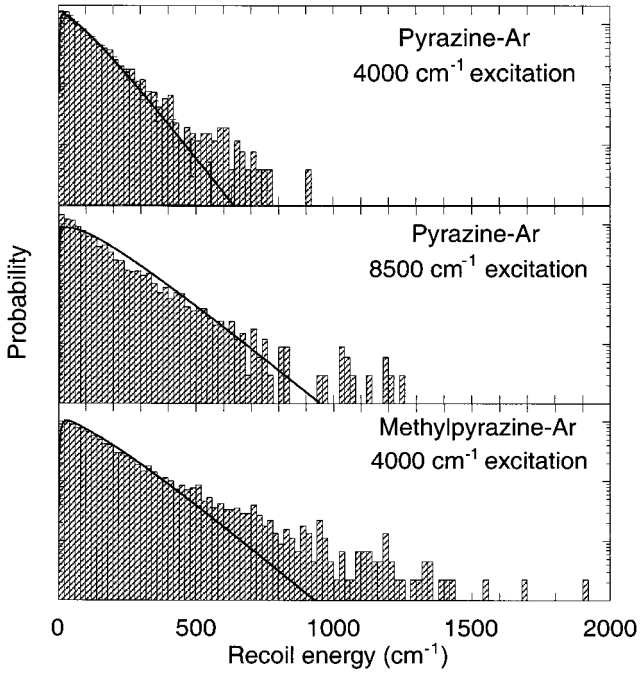

Figure 2. Recoil energy distributions for cluster dissociation. Histograms are from trajectory calculations and lines are from experiments (ref 2). The experimental data in the middle panel are from benzene−Ar dissociation. (See text) Error bars in the top panel are estimated based on reproducibility of repeated measurements. (Note log scale on probability axis.)

The recoil energy distributions for pyrazine−Ar and methylpyrazine−Ar dissociation are shown in Figure 2. Both calculated distributions resemble exponential functions, but with slightly higher probabilities at high energy. In each case, the calculated recoil distribution is in remarkably good agreement with the corresponding experimental data. The interaction potential surfaces of benzene and pyrazine are similar in their well depths and locations, so the calculated recoil of pyrazine−Ar at 8500 cm^{-1} is compared with the experimental data for benzene−Ar. The shapes of the distributions at low recoil energy are reproduced well, but the calculations predict somewhat more intensity in the high energy tail than is observed experimentally; (note also that the experimental uncertainty becomes greater in the high energy tail.) It should be emphasized that the potential energy parameters were not adjusted to achieve the good agreement between experiment and theory. The good quantitative agreement is most likely fortuitous, since the Lennard-Jones potential surface greatly overestimates the well depth, and may have other problems. The most important results are that the

TABLE 4: Calculated Energy Transfer from Dissociation of vdW Clusters (cm^{-1})

cluster	pyrazine−Ar	pyrazine−Ar	methylpyr−Ar
initial vibrational excitation energy	8500	4000	4000
$\langle E_{trans}\rangle$	142 ± 3	114 ± 2	196 ± 3
$\langle E_{trans}\rangle$ experimental[a]	126[b]	95	119
		76	
		86	
$\langle E_{rot}\rangle$	137 ± 3	116 ± 2	183 ± 3
$\langle \Delta E\rangle_{r,t}$	−279 ± 4	−230 ± 4	−379 ± 5
cluster lifetime $\langle\tau\rangle$	81 ± 1 ps	132 ± 2 ps	35 ± 1 ps

[a] Experimental data from ref 2. [b] Experimental $\langle E_{trans}\rangle$ at 8500 cm^{-1} from benzene−Ar data.

overall shapes of the distributions are reproduced well and the experimental trends with vibrational energy and methyl rotor are in agreement.

In the calculation, the pyrazine molecule and argon atom are initially at rest in the center of mass frame, so the initial translational and rotational energies are zero. The average changes in translational and rotational energy are determined by averaging the appropriate product distributions, where the individual quantities are generated by the calculation

$$\langle E_{trans}\rangle = \frac{1}{N}\sum_{i}^{N} E_{trans,i}$$

$$\langle E_{rot}\rangle = \frac{1}{N}\sum_{i}^{N} E_{rot,i} \quad (1)$$

Here, N is the total number of trajectories and E_{trans} is the relative translational energy, which has been separated from the center-of-mass translational energy. All of the trajectories dissociate, so there is no need to consider an "elastic peak", as in the case of collisions. The average vibrational energy transferred to rotational and translational degrees of freedom is

$$\langle \Delta E\rangle_{r,t} = \langle \Delta E_{vib}\rangle_{clus} + \epsilon = -\frac{1}{N}\sum_{i}^{N}(E_{trans,i} + E_{rot,i}) \quad (2)$$

where ϵ is the vdW well depth. In this notation, $\langle \Delta E_{vib}\rangle_{clus}$ refers to the change in the vibrational energy resident in the aromatic partner. Considering only the V→RT energy transfer enables a more direct comparison with the collisional calculations, since full collisions do not require additional vibrational energy to overcome the vdW well depth.

The calculated energy transfer parameters are shown in Table 4 along with the corresponding experimental values. The calculated recoil energies are greater in magnitude than the experimental results, but the overall trends are similar. The increase in vibrational energy from 4000 to 8500 cm^{-1} increases the energy transfer only slightly. Note that the change in total vibrational energy in the calculation is actually from 4000 cm^{-1} + zero point energy to 8500 cm^{-1} + zero point energy, an increase of ∼25%, not a factor of 2. The weak dependence on vibrational energy is consistent with the experimental trend, in which the benzene recoil energy is slightly higher than that of pyrazine.[2] Both the experiments and the calculations indicate that the recoil energy is not strongly dependent on initial energy.

The final rotational energy distributions have not been measured experimentally but are available from the calculations. For each excitation energy, the rotational energy distribution is similar to the corresponding translational energy distribution. All of the distributions resemble exponential functions with high energy tails, and the average rotational energy released in each cluster dissociation is nearly the same as the corresponding average translational energy release (Table 4). This indicates that the energy in the vdW modes is equipartitioned. According to phase space theory and conservation of linear momentum, only two of the three degrees of freedom associated with the relative motion of the products are independent.[24] Similarly, at low rotational energy, the rotational degrees of freedom are reduced by one to account for conservation of angular momentum.[24] In the present situation, the products are an atom and a polyatomic molecule with low rotational energy, so there are two effective translational and two effective rotational degrees of freedom. Each degree of freedom carries 1/2 kT^*, where T^* is an effective canonical temperature that can be found by fitting the product rotational and translational energy distributions to Boltzmann energy distributions.[24]

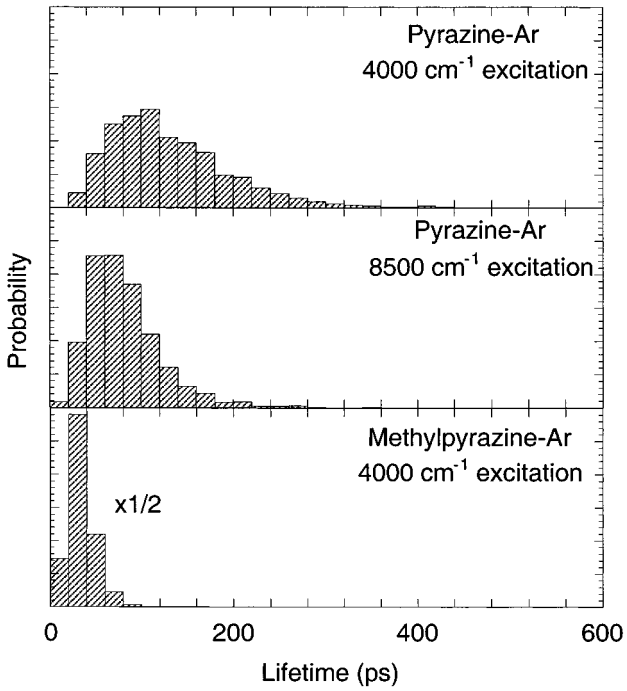

Figure 3. Lifetime distributions for vdW clusters.

The vibrational predissociation lifetimes of these clusters have not been measured experimentally but can be estimated from the calculations. The calculated recoil distribution does not correlate with calculated lifetime for either initial vibrational energy. Bernshtein and Oref reach a similar conclusion on the basis of their benzene−Ar cluster dissociation calculations.[19] The final dissociation kick depends only on the instantaneous vibrational phases of the molecular vibrations, not on past history. The calculated trajectory lifetime distribution for each cluster is shown in Figure 3. The pyrazine clusters with lower initial energy (4000 cm^{-1}) tend to have longer lifetimes than the higher initial energy (8500 cm^{-1}) clusters. At higher vibrational energy, coupling between the molecular modes and vdW modes is enhanced, energy redistribution is faster, and the cluster lifetime is shorter. This result and the "hopping" of argon around the pyrazine molecule point toward a model in which vibrational energy flows from multiple molecular modes to the vdW modes. When enough energy accumulates in the vdW modes, the cluster dissociates. This process is evidenced by the increase in kinetic energy of the argon atom as a function of time, as illustrated in Figure 4. The top panel in the figure shows a typical single trajectory. The oscillations result because

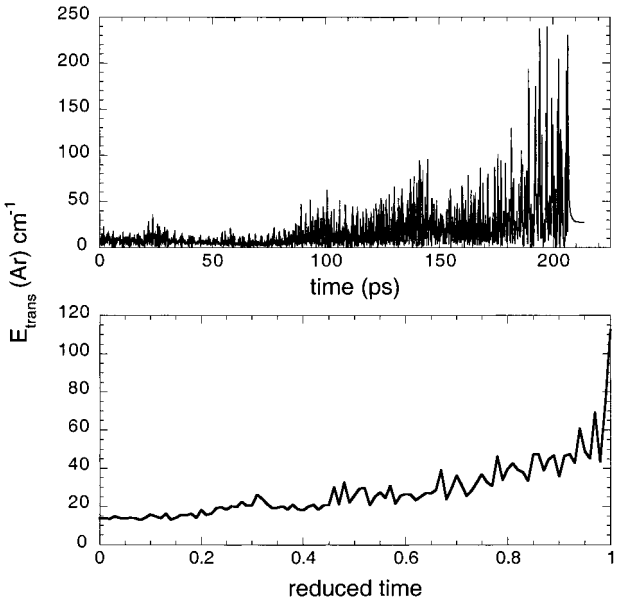

Figure 4. (Upper) Kinetic energy of Ar atom as a function of time for one trajectory. (Lower) 10-trajectory average of kinetic energy of Ar atom as a function of reduced time.

only the kinetic energy is shown, and not the potential energy associated with the vdW modes.

To show a sense of the general trend of energy flow into the vdW modes, the kinetic energy profiles for 10 random trajectories were averaged. Due to the wide variation in trajectory lifetimes, each profile was scaled to a reduced time (defined as the time divided by the trajectory lifetime). The result is shown in the bottom panel of Figure 4. The 10-trajectory sample is not adequate to capture the complete statistics for the process, but it does show the gradual flow of energy into the vdW modes before dissociation. This result differs from that obtained by Bernshtein and Oref on benzene−Ar with ∼52000 cm^{-1} excitation energy, which shows an instantaneous energy kick without a prior buildup of energy in the vdW modes.[19] The different behaviors observed in benzene−Ar and the present results are likely due to the large difference in initial vibrational energy. Additional calculations at intermediate vibrational excitation energies would be necessary to investigate the changeover between mechanisms. This model also differs from one proposed by Ramaekers et al.[25] in which only a single low-frequency, out of plane molecular mode participates in cluster dissociation.

The pyrazine−Ar dissociation calculations may be compared with the work of Bernshtein and Oref on benzene−Ar clusters,[19,26] because of the similarities between the pyrazine−Ar and benzene−Ar potential surfaces. They find the average trajectory lifetime to be 36.3 ps for 51900 cm^{-1} excitation and 94.2 ps for 30864 cm^{-1} excitation. This trend of increasing lifetime with decreasing internal energy is consistent with our results. A more direct comparison between our results and those of Bernshtein and Oref cannot be made, since their criteria for terminating trajectories and assumed initial excitation conditions differ from ours.

Methylpyrazine−Ar Cluster Dissociation. The addition of a methyl rotor changes the vdW molecular mode couplings in several ways. At the vibrational energy described here, the rotor is hindered, so it behaves more like a low-frequency vibration (∼170 cm^{-1}).[15] In addition to its contribution to the density of states, it has an out-of-plane component and so it may enhance interactions with the out-of-plane vdW modes. To examine these effects on cluster dissociation, calculations were performed on methylpyrazine−Ar with initial excitation energy of 4000 cm^{-1}. The density of states (ρ) at this energy in methylpyrazine is 40 times greater than in pyrazine ($\rho = 4 \times 10^4$/cm^{-1} and 10^3/cm^{-1}, respectively). The cluster lifetime dramatically decreases with the addition of the methyl rotor (Table 4 and Figure 3). A possible explanation of this effect is the increased mode coupling induced by the methyl torsion, which enables the energy to flow quickly into the out-of-plane vdW modes. The resulting product energy distribution, however, is not strongly affected by the increased rate of energy flow. The average recoil energy calculated for dissociation of methylpyrazine−Ar clusters is listed in Table 4, along with the corresponding experimental values. In both the predissociation experiments and calculations, the addition of the methyl rotor increases the energy transfer only moderately. The methyl rotor effect is more pronounced in the calculated recoil energy (∼65% increase) compared with the experiments (∼40% increase).

These results may be compared with those from collisional deactivation experiments on the effect of the methyl rotor. Wu and Weisman[27] found that T_1 methylpyrazine was ∼50% more efficiently deactivated by argon than was T_1 pyrazine. This trend is consistent with the T_1 cluster predissociation experimental data[2] and the present calculations. In collisional deactivation experiments, the differences due to the presence of a methyl rotor become more pronounced as vibrational energy increases. In collisions involving S_0 benzene[28] and S_0 toluene[29] containing ∼8500 cm^{-1}, toluene has a slightly higher average energy transfer per collision; however, at 24 000 cm^{-1}, toluene is deactivated more than three times more efficiently than benzene for argon collider. Linhananta and Lim[30] found similar energy-dependent effects in trajectory calculations on ethane and concluded that the methyl internal rotor in ethane significantly increased collisional energy transfer at high vibrational energy. However, at low vibrational energy, the rotor is hindered and the enhancement of collisional energy transfer is diminished. This is the expected situation in the present work, in which the methyl rotor is hindered.

Pyrazine−Ar Collisions. In the collisional calculations, the internal energy, which is rigorously conserved in the absence of collisions, includes both the vibrational and rotational energy in addition to the zero point energy. In many cases, the results of collisional trajectory studies have been reported in terms of internal energy transfer.[4,10,17] This quantity is easily available from the calculation output. However, experiments on large molecule energy transfer are sensitive only to changes in vibrational energy.[31−33] To compare our trajectory results with experimental results, the vibrational energy must be separated from the rotational energy.[5] The rotational energy, E_{rot}, is determined approximately by means of the angular momentum, J, which is also a rigorously conserved quantity in the absence of collisions

$$E_{rot} = \frac{J^2}{2(I_A I_B I_C)^{1/3}} \tag{3}$$

where I_A, I_B, and I_C are the moments of inertia. To find the approximate average vibrational energy transfer, $\langle \Delta E_{vib} \rangle_{traj}$, the rotational energy transfer is subtracted from the total energy transfer, E, and the average is taken over all trajectories, N

$$\langle \Delta E_{vib} \rangle_{traj} = \frac{1}{N} \sum_{i}^{N} (\Delta E_i - \Delta E_{rot,i}) \tag{4}$$

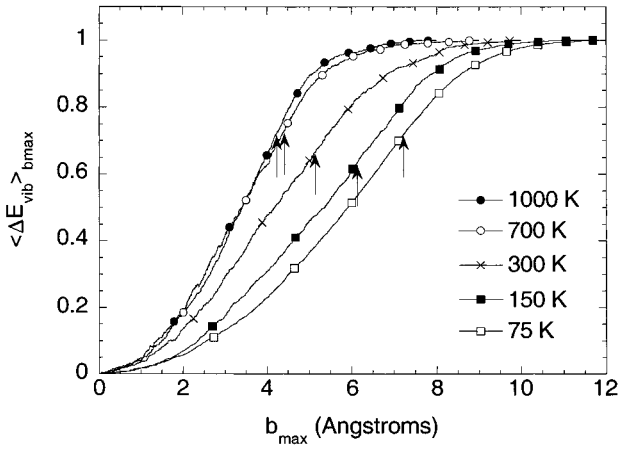

Figure 5. Integrated vibrational energy transfer as a function of b_{max} at different temperatures. The energy axis is relative to the converged value at each temperature. The arrows show the experimental Lennard-Jones collision radius.

The above average includes "uninteresting" trajectories that result from high impact parameter collisions. To account for the effects of uninteresting collisions, the average obtained from the set of trajectories, $\langle \Delta E_{vib} \rangle_{traj}$ is scaled by the ratio $\pi b_{max}^2/\pi b_{eff}^2$, where b_{eff} is an effective collision radius.[34,35] Generally, the Lennard-Jones collision radius (b_{LJ}) has been used in place of b_{eff} in the above ratio to scale the trajectory results, with $b_{LJ} = \sigma_{LJ}\sqrt{\Omega^{2,2}*}$ where σ_{LJ} is the average Lennard-Jones radius and $\Omega^{2,2}*$ is the collision integral, which depends on temperature. However, the Lennard-Jones parameters (and the associated temperature dependence of $\Omega^{2,2}*$) are not known for the present model potential. Moreover, the Lennard-Jones collision radius is spherically symmetric, but at low temperatures the asymmetry of pyrazine becomes more important and may affect the effective collision radius.[36] Because the temperature dependence is an important part of this work, we obtain b_{eff} for each temperature in an internally consistent way from the trajectory results. For each set of trajectories, b_{eff} is found in the following way. The cumulative vibrational energy transfer $\langle \Delta E_{vib} \rangle_{bmax}$ is plotted as a function of b_{max} as in Figure 5

$$\langle \Delta E_{vib} \rangle_{bmax} = \frac{1}{N_{bmax}} \sum_{i}^{N_{bmax}} (\Delta E_i - \Delta E_{rot,i})\; b \le b_{max} \quad (5)$$

where N_{bmax} is the number of trajectories with $b \le b_{max}$. The energy axis in Figure 5 represents the cumulative vibrational energy relative to the limiting value at each temperature. For eq 5 to be valid, the impact parameters for each set of trajectories must be chosen from the appropriate statistical distribution: $f(b) = 2b\, db/b_{max}^2$.[23] As can be seen in Figure 5, the vibrational energy transfer convergence depends on temperature. Low-temperature collisions have a larger cross section than high-temperature collisions due to the attractive vdW potential. The arrows in Figure 5 show the experimental Lennard-Jones collision radius (estimated from measured critical constants) at each temperature. From Figure 5 it is clear that the calculated cross section for vibrational energy transfer has the same temperature dependence, but is larger than that estimated from the experimental Lennard-Jones parameters. At the Lennard-Jones radius, $\langle \Delta E_{vib} \rangle_{bmax}$ reaches 65 to 75% of its limiting value. We chose the radius corresponding to 70% of the limiting value of $\langle \Delta E_{vib} \rangle_{bmax}$ for b_{eff}. The 70% value is arbitrary and serves only to allow comparison with other trajectory results or experimental data that are based on the experimental Lennard-Jones collision frequency.

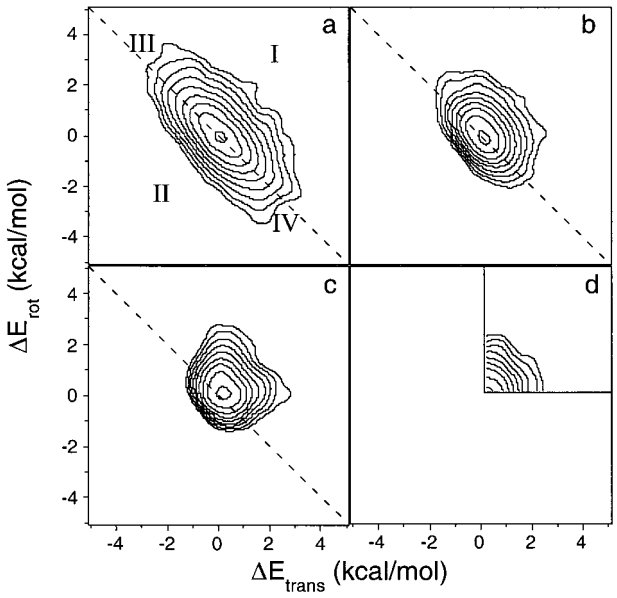

Figure 6. Step-size probability contour plots for pyrazine−Ar energy transfer. (a) 300 K; (b) 150 K; (c) 75 K, (d) vdW cluster. The highest probability contour is in the center, and each succeeding contour has half the value of the previous contour.

TABLE 5: Temperature Dependence of Collisional Energy Transfer

	$\langle \Delta E_{trans} \rangle$	$\langle \Delta E_{rot} \rangle$	$\langle \Delta E_{vib} \rangle$	$-\langle \Delta E_{vib} \rangle_d$
4000 cm^{-1}				
1000 K	-13 ± 12	41 ± 12	-30 ± 7	519 ± 10
300 K	27 ± 2	33 ± 2	-61 ± 2	240 ± 3
150 K	39 ± 2	50 ± 2	-89 ± 2	230 ± 3
75 K	63 ± 1	76 ± 2	-139 ± 2	257 ± 3
cluster	114 ± 2	116 ± 2	-230 ± 4	230 ± 4
8500 cm^{-1}				
300 K	40 ± 4	46 ± 4	-87 ± 4	301 ± 5
24000 cm^{-1}				
1000 K	80 ± 11	115 ± 11	-195 ± 9	853 ± 14
700 K	106 ± 10	120 ± 10	-227 ± 9	773 ± 15
300 K	104 ± 5	100 ± 5	-204 ± 5	505 ± 9
75 K	159 ± 3	173 ± 3	-332 ± 4	537 ± 6

The average energy transfer parameters are scaled using the relationship

$$\langle \Delta E_{vib} \rangle = \frac{\pi b_{max}^2}{\pi b_{eff}^2} \langle \Delta E_{vib} \rangle_{traj} \quad (6)$$

The expression for $\langle \Delta E_{vib} \rangle$ in eq 6 includes contributions from both activating and deactivating collisions. The average energy transferred in deactivating collisions $\langle \Delta E_{vib} \rangle_d$ provides information about the width of the step-size probability distribution. These scaled energy transfer quantities are listed in Table 5 for pyrazine−Ar collisions at each temperature and excitation energy.

The probability density distributions for energy transfer are displayed as contour plots in Figure 6. The highest probability is due to the elastic peak at (ΔE_{trans}, ΔE_{rot}) $\approx$ (0,0). Starting at the center, each contour represents half the intensity of the previous contour, so equally spaced contours indicate an exponential variation. The dashed diagonal line corresponds to $\Delta E_{rot} = -\Delta E_{trans}$, or $\Delta E_{vib} = 0$. To the right and above the dashed line (Area I) is the probability distribution for vibrational deactivation, while the area below and to the right of the dashed

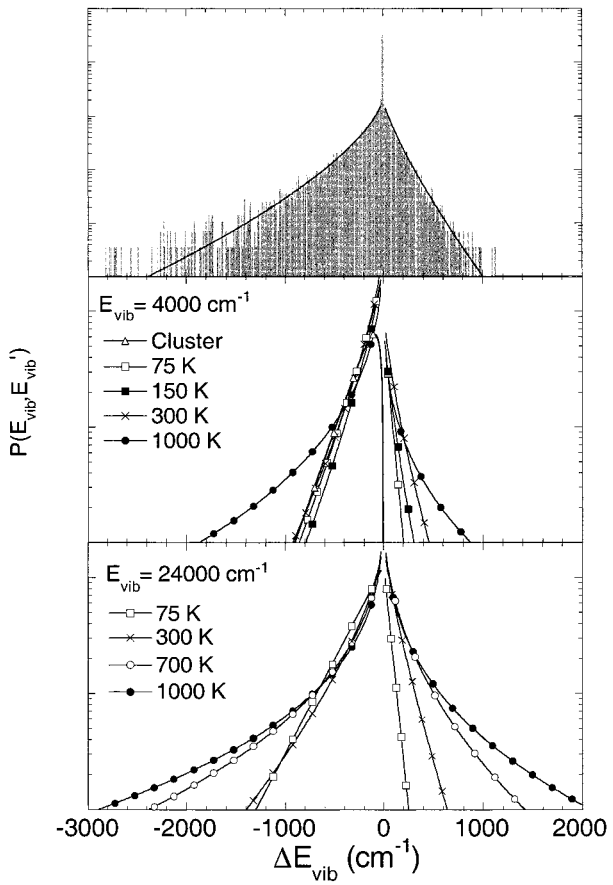

Figure 7. Vibrational energy step-size probability histograms as a function of temperature and initial excitation energy. The upper panel shows the histogram from the 300 K, 24 000 cm^{-1} data set to demonstrate the quality of the least-squares fits. In the center and lower panels, the elastic peaks are not shown. (Note log scales on probability axes.)

line (Area II) represents vibrational activation. The distance from the diagonal line corresponds to the vibrational energy transfer step size. The probability density at 300 K tends to lie along the dashed line; this indicates a tendency for vibrationally elastic collisions. However, even collisions that do not transfer vibrational energy can exchange rotational and translational energy. This is indicated in Figure 6a by Areas III and IV, the R−T transfer "wings". As temperature decreases, the proportion of collisions which exchange R−T energy decreases, and the "wings" shrink (Figure 6b and c). This is because the effective potential for the collision changes with temperature. Bernshtein and Oref[36] calculated dynamic global potentials for collisions using benzene−Ar classical trajectories. They found that at high temperatures the effective potential is approximately spherical with a shallower well depth, because the molecule is rapidly rotating. The lowest potential region is not accessible to the argon atom because it is shielded by the hydrogen atoms of the rotating molecule. Collisions in this regime favor R−T energy exchange. As temperature decreases, the lower rotational and translational energies allow the argon atom to approach the deeper attractive region of the potential.[36] In this situation V−RT energy transfer becomes more probable.

The vibrational step size distribution functions, $P(E_{vib},E'_{vib})$ at $E_{vib} = 4000$ and 24000 cm^{-1} are shown in Figure 7 for each temperature. The trajectories were binned according to vibrational energy transfer step size; 10 cm^{-1} bins were chosen because this is a common bin size in master equation simulations.[37] Numerous attempts have been made in trajectory studies

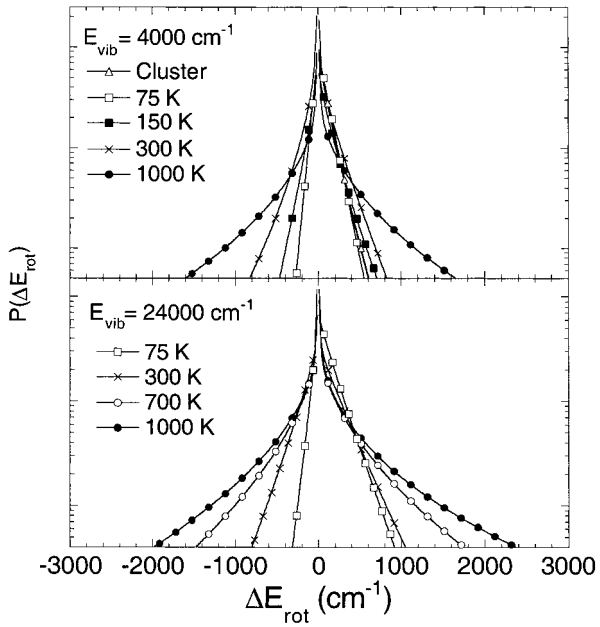

Figure 8. Rotational energy step-size probability histograms as a function of temperature and initial excitation energy. The elastic peaks are not shown. (Note log scales on probability axes.)

to account for the elastic peak at $\Delta E = 0$ and obtain quantitatively accurate fits to $P(E,E')$.[5,38−40] In this work, both wings of the histograms were least-squares fitted to the following functional form:

$$P(E_{vib},E'_{vib}) = A \exp\left[-\left(\frac{|E_{vib} - E'_{vib}|}{\alpha}\right)^{Y}\right] \qquad (7)$$

where $\alpha = C_0 + C_1E_{vib}$. This functional form has been suggested by Luther and co-workers[41] based on their experimental collisional energy transfer results. In the present work, the histogram points (except for the elastic peak at ±5 cm^{-1}) were fitted to eq 7 by nonlinear least squares. For pyrazine−Ar collisions at 24 000 cm^{-1} excitation, the fitted parameters for down steps are $\alpha = 97$ cm^{-1} and $Y = 0.63$, in rough agreement with the toluene−Ar experimental result:[41] $\alpha = 144$ cm^{-1} and $Y = 0.70$. The histogram for 300 K collisions at 24 000 cm^{-1} excitation is shown in the upper panel of Figure 7, along with the least-squares fit to eq 7. The fitted probability histograms for each temperature and excitation energy are shown in the lower panels of Figure 7. At 4000 cm^{-1} excitation and temperatures below 300 K, $\langle\Delta E_{vib}\rangle_d$ does not vary with temperature. This is also evident in Figure 6a−c, where the portion of the probability distribution in Area I is similar for each temperature. At temperatures above 300 K, the situation changes. The probability for weak ($< \sim$400 cm^{-1}) downward collisions is nearly independent of temperature, but the high energy tail of the distribution is enhanced at higher temperatures, and $\langle\Delta E_{vib}\rangle_d$ increases (Table 5). This suggests that the energy transfer mechanism changes around 300 K for this potential surface. At higher temperatures, collisions which transfer very large energies (sometimes referred to as "supercollisions"[42−45]) become more probable.

The calculated rotational step-size distributions at $E_{vib} = 4000$ and 24000 cm^{-1} are shown in Figure 8. The rotational histograms were least-squares fitted either with eq 7 or with the sum of eq 7 and another exponential term. The second term was necessary for the higher temperature histograms. Upward transitions are favored slightly because the vibrational "temperature" is higher than the rotational temperature. As in the

vibrational step-size distributions, the behavior of the rotational step-size distribution at low temperature is different than at high temperature. At ~300 K and lower, the distribution for rotationally activating collisions becomes independent of temperature. At higher temperatures, the probability increases for collisions that exchange large amounts of rotational energy.

The Relationship between Clusters and Collisions. In the limit of low temperature, the initial translational and rotational energies approach zero, and the collision interaction approaches that of vdW cluster predissociation. In order for a vdW cluster to dissociate, vibrational energy must flow from the molecule into the vdW modes until the potential energy well is "filled." Upon dissociation of the cluster, excess energy in the vdW modes correlates with the final recoil and rotational energy. Of the initial vibrational energy E_{vib}, ϵ is used to overcome the potential well, and $E_{vib} - \epsilon$ is available for redistribution in the products. (Note that only a small fraction of this available energy actually ends up in the products' recoil and rotations.) In the case of a collision, the total vibrational energy available for redistribution is $E_{vib} + E_{trans}$. The small difference in available vibrational energy for the cluster dissociation and the collision, equal to $\epsilon + E_{trans}$, is not likely to affect the resulting Δ(T,R) product state distributions because the energy dependence is weak, as described above.

To compare the energy transfer in cluster predissociation with that in collisions, a contour plot from pyrazine−Ar predissociation is displayed in Figure 6d. In this representation, only the V→T,R product distributions are considered; ϵ is not included. Only one quadrant in Figure 6d contains data because the translations and rotations were initially cold. The distribution within that quadrant, however, is very similar to the collisional distributions. The cluster step size distribution is shown with the collisional results at 4000 cm^{-1} in Figure 7 and Figure 8. The cluster distribution does not contain an elastic peak, so it is not normalized to the same area as the collisional distributions. It has been scaled in order emphasize that the slope of the distribution for cluster dissociation is nearly the same as for the low temperature (<300 K) collisions. This fact indicates that the product Δ(T, R) energy transfer distribution from vibrational predissociation of the cluster is a good approximation to the final Δ(T, R) energy distribution in full collisions, when the polyatomic is excited to essentially the same initial vibrational energy. The step-size probability distribution obtained from cluster dissociation shown in Figure 7 is not the same as the full $P(E,E')$ for vibrational energy transfer, because it includes only vibrational energy transferred to rotations and translations, and not the vibrational energy used to overcome the vdW binding energy, which is the lower limit for vibrational energy transfer.

There are other fundamental differences between vdW cluster dissociation and collisional energy transfer that must be recognized when comparing these results. The initial cluster orientation is constrained to the particular geometry corresponding to the deepest well on the potential surface. Collision partners, on the other hand, approach each other with all orientations. This difference may not be important for vibrational energy transfer, however, because during the period when vibrational energy is flowing from the aromatic molecule to the vdW modes in a cluster, the argon atom moves among the wells on the potential surface and samples many orientations. When the final dissociation kick occurs, the argon atom is not necessarily in the lowest potential position. Indeed, in all ~20 trajectories that were examined individually in the present work, the dissociation never occurred from the equilibrium position.

Comparison with Other Work. The results indicate that at low temperature $\langle \Delta E_{vib} \rangle_d$ is nearly independent of temperature. These results are consistent with experiments in which vibrationally excited pyrazine is deactivated by unexcited pyrazine:[9] $\langle \Delta E_{vib} \rangle_d$ is nearly constant over the 250−425 K temperature range. At the lower temperatures (250−300 K) $\langle \Delta E_{vib} \rangle_d$ increases slightly; this has been attributed to enhanced V−V energy transfer,[9] which does not occur in Ar collisions. Other experimental work on collisional energy transfer has also indicated a weak temperature dependence.[6−9]

The temperature dependence of vibrational energy transfer has been assessed in trajectory calculations for collisions between azulene and Xe,[10] benzene and Ar,[5,40] hexafluorobenzene and Ar,[5] and toluene and He.[11] In all cases, the calculated temperature dependence is weak. In thermal (T_{trans} = 904 K, E_{vib} = 6300 cm^{-1}) benzene−Ar collisions,[40] as the rotational temperature increases from 300 to 900 K, $\langle \Delta E_{vib} \rangle$ remains constant while the absolute value of $\langle \Delta E_{vib} \rangle_d$ increases from ~50 to ~150 cm^{-1}. The same effect is calculated in highly excited benzene−Ar collisions[5] (T_{trans} = 300 K, E_{vib} = 24000 cm^{-1}): $\langle \Delta E_{vib} \rangle$ is ~ −30 cm^{-1} as T_{rot} varies from 300 to 500 K. These calculated results are in agreement with the present results for temperatures greater than 300 K at the higher excitation energy. At lower excitation energy and lower temperature, $\langle \Delta E_{vib} \rangle_d$ is calculated to converge to a constant value and $\langle \Delta E_{vib} \rangle$ varies.

In comparison with experiments on S_0 pyrazine collisions,[46] the calculated energy transfer parameters are too large by approximately a factor of 5 for argon collider, while the overall functional form (linear dependence on vibrational energy) is reproduced. This overestimation of energy transfer has been noticed in other work when pairwise Lennard-Jones potentials were used to construct the intermolecular potential.[4] One reason for this effect is that the Lennard-Jones well depth is too large by a factor of ~2. For argon collisions, $\langle \Delta E \rangle$ is strongly dependent on well depth, except at very high temperatures where $kT \gg \epsilon$. Potentials with the correct well depth produced quantitative simulations of toluene−Ar energy transfer.[4]

Energy Transfer in Singlet and Triplet States. Experimentally there is a large difference between collisional energy transfer in the S_0 and T_1 states of pyrazine.[47,46] The deactivation of pyrazine with E_{vib} = 5000 cm^{-1} by argon is ~20 times as efficient as in the ground state. One explanation for this is the softening of the vibrational modes of pyrazine in the excited state. The pyrazine out-of-plane torsional mode frequencies decrease from 420 and 341 cm^{-1} in the S_0 state[14] to 406 and 237 cm^{-1}, respectively, in the T_1 state.[48] The effect of this change on the dissociation of pyrazine−Ar was investigated by decreasing the force constants in the pyrazine intramolecular potential to give the lower vibrational frequencies. With this new potential, the average recoil energy increased from 114 to 160 cm^{-1}. It appears that the lowering of vibrational frequencies increases the coupling to the van der Waals modes, and as a result more energy is released in the recoil of the products. The geometry and polarizability of the molecule are also likely to be different in the excited state. The excited-state polarizability is expected to be higher than in the ground state, increasing the vdW well depth. A deeper well would promote coupling between the molecular modes and the vdW modes, and energy transfer would be enhanced.

To obtain good quantitative agreement among predissocation experiments, collisional experiments, and trajectory calculations, changes will be necessary in the potential surface. First, the intramolecular surface with "softer" T_1 frequencies should be used in the predissociation calculations. Second, the correct

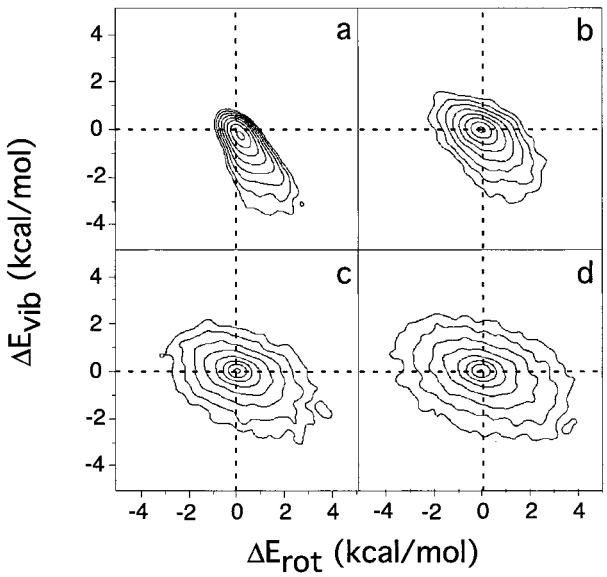

Figure 9. Step-size probability contour plots for pyrazine−Ar energy transfer. (a) 75 K; (b) 300 K; (c) 700 K; (d) 1000 K. The highest probability contour is in the center, and each succeeding contour has half the value of the previous contour.

intermolecular well depth should be used. Implementing the T_1 vibrational frequencies and a more realistic, shallower intermolecular potential have opposite effects on the energy transfer, so cancellation of errors may explain the good quantitative agreement with the experimental cluster predissociation data found with the present potential. The shallower well with the use of S_0 frequencies would likely bring the collisional results more in line with the experimental S_0 data.

Implications for Master Equation Modeling. Master equation simulations are useful in modeling collisional energy transfer. For systems in which transfer of angular momentum as well as vibrational energy are important, a 2-dimensional master equation is necessary. Functional forms that have been suggested for the step-size distribution generally assume that the rotational and vibrational energy transfer probability distributions are separable:[38,49]

$$P(E,J,E',J') = P(E_{vib},E'_{vib})P(E_{rot},E'_{rot}) \quad (8)$$

To test if this assumption is appropriate, the correlation between ΔE_{vib} and ΔE_{rot} can be determined from trajectory calculations, based on the approximate separation of rotational and vibrational energy in eq 5. The joint step-size probability distributions are shown in Figure 9 for pyrazine−Ar collisions with $E_{vib} = 24\,000$ cm^{-1} at four different temperatures. The highest probability is in the center, and each succeeding contour represents half the intensity of the previous contour. The degree to which each contour plot appears to deviate from horizontal and vertical bilateral symmetry gives a qualitative measure of the correlation between vibrational and rotational energy transfer. The lowest temperature (75 K) shows the strongest correlation: in Figure 9a, the tail toward the lower right corresponds to transfer from vibration to rotation. As temperature increases, there is less correlation. Therefore, a model such as eq 8 may be adequate for high-temperature simulations, but will be less accurate at low temperatures.

These results are similar to those obtained by Schranz and Troe[38] in their trajectory studies on collisional deactivation of SO_2. They fitted the 2-dimensional step-size probability functions to eq 8 using exponential functions for the separate E_{vib} and E_{rot} distributions. They found that these functions were inadequate in that they did not capture all the details of the distribution due to correlation between rotational and vibrational energy transfer. Another 2-dimensional function that has been used in master equation simulations is a completely uncorrelated model in which either the vibrational or rotational energy can change during a collision, but not both.[49] In a contour plot representation such as Figure 9, this model predicts that all trajectories would fall on the principal axes, shown as dashed lines in the figure. This model is clearly inconsistent with the trajectory data. Further work along these lines is necessary for implementation of 2-D master equation simulations.

Conclusions

Classical trajectory calculations using a simple model potential constructed from pair-wise Lennard-Jones functions are found to be capable of modeling the main features of the recoil distributions from vibrational predissociation of aromatic−Ar vdW clusters. The overall shape of the recoil distributions, a smooth exponential function with maximum probability for zero recoil, is in good agreement with the experimental work. In addition, the trends evident in the experiments are also simulated well: increasing the vibrational energy or adding a methyl group to the donor molecule produces a modest increase in average recoil energy.

The calculations predict that the cluster lifetime depends strongly on the vibrational energy and the presence of a methyl group, which appears to increase coupling between the molecular modes and the vdW modes and increase the rate of energy flow. When enough energy is present in the vdW modes to overcome the binding energy, the cluster dissociates, and the energy remaining in the molecular modes has little effect on the final rotational and translational energies. The cluster lifetimes may be experimentally measurable; such experiments would be able test this qualitative cluster predissociation model.

Collisional energy transfer and vibrational predissociation of vdW clusters are related to each other through their temperature dependence. At temperatures lower than ~300 K, $P(E,E')$ (at 4000 cm^{-1} vibrational energy) for deactivating collisions converges to an approximately exponential function that is independent of temperature. The cluster dissociation product distribution (for V−RT energy transfer) resembles the limiting low-temperature distribution. This indicates that a similar mechanism controls energy transfer in low-temperature collisions and in vdW cluster predissociation. Therefore, experimental work on cluster predissociation may serve to inform our understanding of collisional energy transfer.

Acknowledgment. Thanks go to Dr. Dave Chandler and Dr. Thomas Lorenz for helpful discussions. Financial support was provided in part by the U.S. Department of Energy, Office of Basic Energy Sciences. L.M.Y. thanks the Horace H. Rackham School of Graduate Studies for a Predoctoral Fellowship. J.R.B. thanks Prof. William L. Hase and the Chemistry Department at Wayne State University for their hospitality during a sabbatical visit.

References and Notes

(1) Yoder, L. M.; Barker, J. R.; Lorenz, K. T.; Chandler, D. W. *Chem. Phys. Lett.* **1999**, *302*, 602.
(2) Yoder, L. M.; Barker, J. R. *Phys. Chem. Chem. Phys.* **2000**, *2*, 813.
(3) Bruehl, M.; Schatz, G. C. *J. Phys. Chem.* **1988**, *92*, 7223.
(4) Lim, K. F. *J. Chem. Phys.* **1994**, *100*, 7385.
(5) Lenzer, T.; Luther, K.; Troe, J.; Gilbert, R. G.; Lim, K. F. *J. Chem. Phys.* **1995**, *103*, 626.
(6) Heymann, M.; Hippler, H.; Troe, J. *J. Chem. Phys.* **1984**, *80*, 1853.

(7) Barker, J. R.; Golden, R. E. *J. Phys. Chem.* **1984**, *88*, 1012.
(8) Miller, L. A.; Cook, C. D.; Barker, J. R. *J. Chem. Phys.* **1996**, *105*.
(9) Brown, T. C.; Taylor, J. A.; King, K. D.; Gilbert, R. G. *J. Phys. Chem.* **1983**, *87*, 5214.
(10) Lim, K. F. *J. Chem. Phys.* **1994**, *101*, 8756.
(11) Clarke, D. L.; Oref, I.; Gilbert, R. G.; Lim, K. F. *J. Chem. Phys.* **1992**, *96*, 5983.
(12) Hase, W. L.; Duchovic, R. J.; Hu, X.; Komornicki, A.; Lim, K. F.; Lu, D.-H.; Peslherbe, G. H.; Swamy, K. N.; VandeLinde, S. R.; Varandas, A.; Wang, H.; Wolf, R. J. *J. Quantum Chem. Program Exchange Bull.* **1996**, *16*, 43 [QCPE Program 671].
(13) Lim, K. F.; Gilbert, R. G. *J. Phys. Chem.* **1990**, *94*, 77.
(14) Zarembowitch, J.; Bokobza-Sebagh, L. *Spectrochim. Acta A* **1976**, *32*, 605.
(15) Arenas, J. F.; Lopez-Navarrete, J. T.; Marcos, J. I.; Otero, J. C. *J. Chem. Soc., Faraday Trans. 2* **1988**, *84*, 53.
(16) Watanabe, T.; Shimada, H.; Shimada, R. *Bull. Chem. Soc. Jpn.* **1982**, *55*, 2564.
(17) Bernshtein, V.; Lim, K. F.; Oref, I. *J. Phys. Chem.* **1995**, *99*, 4531.
(18) Wanna, J.; Bernstein, E. R. *J. Chem. Phys.* **1985**, *84*, 927.
(19) Bernshtein, V.; Oref, I. *J. Chem. Phys.* **2000**, *112*, 686.
(20) Freed, K. F. In *Radiationless Processes in Molecules and Condensed Phases*; Fong, F. K., Ed.; Springer-Verlag: Berlin, 1976; Vol. 15; p 23.
(21) Knee, J.; Johnson, P. *J. Phys. Chem.* **1985**, *89*, 948.
(22) Duncan, M. A.; Dietz, T. G.; Liverman, M. G.; Smalley, R. E. *J. Phys. Chem.* **1981**, *85*, 7.
(23) Porter, R. N.; Raff, L. M. In *Dynamics of Molecular Collisions*; Miller, W. H., Ed.; Plenum: New York, 1976; Vol. B.
(24) Baer, T.; Hase, W. L. *Unimolecular Reaction Dynamics. Theory and Experiments*; Oxford University Press: New York, 1996.
(25) Ramaekers, J. J. F.; vanDijk, H. K.; Langelaar, J.; Rettschnick, R. P. H. *Faraday Discuss. Chem. Soc.* **1983**, *75*, 183.
(26) Bernshtein, V.; Oref, I. *Chem. Phys. Lett.* **1999**, *300*, 104.
(27) Wu, F.; Weisman, R. B. *J. Chem. Phys.* **1999**, *110*, 5047.
(28) Yerram, M. L.; Brenner, J. D.; King, K. D.; Barker, J. R. *J. Phys. Chem.* **1990**, *94*, 6341.
(29) Toselli, B. M.; Brenner, J. D.; Yerram, M. L.; Chin, W. E.; King, K. D.; Barker, J. R. *J. Chem. Phys.* **1991**, *95*, 176.
(30) Linhananta, A.; Lim, K. F. *Phys. Chem. Chem. Phys.* **1999**, *1*, 3467.
(31) Barker, J. R.; Toselli, B. M. *Int. Rev. Phys. Chem.* **1993**, *12*, 305.
(32) Hippler, H.; Troe, J.; Wendelken, H. J. *J. Chem. Phys.* **1983**, *78*, 6709.
(33) Hold, U.; Lenzer, T.; Luther, K.; Reihs, K.; Symonds, A. C. *J. Chem. Phys.* **2000**, *112*, 4076.
(34) Lim, K. F.; Gilbert, R. G. *J. Chem. Phys.* **1990**, *92*, 1819.
(35) Gilbert, R. G.; Smith, S. C. *Theory of Unimolecular and Recombination Reactions*; Blackwell Scientific: Oxford, 1990.
(36) Bernshtein, V.; Oref, I. *J. Phys. Chem. A* **2000**, *104*, 706.
(37) Ortiz, N. F.; Barker, J. R., in preparation.
(38) Schranz, H. W.; Troe, J. *J. Phys. Chem.* **1986**, *90*, 6168.
(39) Lendvay, G.; Schatz, G. C. *J. Phys. Chem.* **1994**, *98*, 6530.
(40) Bernshtein, V.; Oref, I. *J. Chem. Phys.* **1998**, *108*, 3543.
(41) Lenzer, T.; Luther, K.; Reihs, K.; Symonds, A. C. *J. Chem. Phys.* **2000**, *112*, 4090.
(42) Oref, I. In *Advances in Chemical Kinetics and Dynamics*; Barker, J. R., Ed.; JAI: Greenwich, 1995; Vol. 2B.; p 285.
(43) Lendvay, G.; Schatz, G. C. *J. Phys. Chem.* **1990**, *94*, 8864.
(44) Bernshtein, V.; Oref, I. *J. Phys. Chem.* **1993**, *97*, 12811.
(45) Mullin, A. S.; Michaels, C. A.; Flynn, G. W. *J. Chem. Phys.* **1995**, *102*, 6032.
(46) Miller, L. A.; Barker, J. R. *J. Chem. Phys.* **1996**, *105*, 1383.
(47) Bevilacqua, T. J.; Weisman, R. B. *J. Chem. Phys.* **1993**, *98*, 6316.
(48) Tomer, J. L.; Holtzclaw, K. W.; Pratt, D. W.; Spangler, L. H. *J. Chem. Phys.* **1988**, *88*, 1528.
(49) Robertson, S. H.; Pilling, M. J.; Gates, K. E.; Smith, S. C. *J. Comput. Chem.* **1997**, *18*, 1004.